

On the Need for Spatial Random Effects in Bayesian Regression Models for Multilevel Areal Data

Shuqi Lin¹ Joshua L. Warren^{*,1}

¹Department of Biostatistics, Yale School of Public Health, New Haven, CT, USA

*joshua.warren@yale.edu

Although spatial models for areal data are widely used in multilevel settings, the conditions under which spatial and nonspatial random effects yield equivalent posterior inference for regression coefficients have never been formally characterized. We address this question within a hierarchical Bayesian framework for Gaussian outcomes, using the Leroux conditional autoregressive (CAR) prior distribution as a representative specification. We derive a closed-form sample size threshold, m^* , below which spatial modeling materially affects inference on regression coefficients and above which a simpler nonspatial model yields effectively equivalent results, and show that the absolute relative difference in posterior variances converges to zero at rate $O(m^{-1})$. The threshold depends on three interpretable quantities: the spatial correlation parameter, the ratio of between-area to within-area variance, and the alignment between the covariate and dominant spatial patterns in the data. Because each can often be estimated prior to model fitting, m^* can serve as a practical study design tool. Simulation studies confirm that m^* accurately identifies this threshold across a range of settings. However, when the covariate does not vary within a given location, spatial modeling remains necessary regardless of within-area sample size. These results offer formal guidance for practitioners deciding whether the added complexity of spatial modeling is warranted.

Key words: Areal data, Bayesian inference, conditional autoregressive model, multilevel modeling, spatial statistics

1. Introduction

Spatially referenced data arise routinely across the health, environmental, and social sciences (Banerjee et al. 2003, Cressie 2015). Observations from nearby locations are often correlated due to shared environmental conditions, social interactions, or other unmeasured factors. Ignoring spatial dependence can lead to underestimated measures of uncertainty (e.g., standard errors, posterior standard deviations), and therefore, inflated type I error rates (Legendre 1993, Dormann et al. 2007).

This has motivated a large body of methods development work on statistical modeling that explicitly incorporates spatial dependence structure (Banerjee et al. 2003, Cressie 2015). Typically, these models introduce location-specific random effects with a correlation structure defined broadly by distances between the spatial units, where the meaning of distance differs based on the type of spatial data (e.g., point-referenced, areal/lattice). This structure allows for information sharing

across spatially proximate random effects, leading to more stable local estimates that would otherwise be too noisy to support reliable inference on their own. As a result, spatial modeling has become a default analytical choice for spatially referenced data.

The majority of spatial models for areal data were developed in settings where each region contributes a single observation, as in disease mapping studies where region-level disease counts are the primary outcome (Besag et al. 1991, Leroux et al. 2000). However, when working with multilevel data, it is common to have multiple observations nested within the same spatial region and to introduce a model at the level of the individual. Random effects are then included primarily to account for clustering among individuals from the same region. In this setting, it is not clear what role a spatially structured random effect plays relative to a simpler nonspatial random effect.

In the absence of formal guidance, current practice has been somewhat inconsistent. Several multilevel studies have incorporated spatially structured area-level effects using conditional autoregressive (CAR) random effects (Dong et al. 2016, Clark et al. 2021, Asare et al. 2022, Bravo et al. 2022, Djeudeu et al. 2022, Cars et al. 2025, Li et al. 2025), and alternative regularization strategies have also been considered (Choi et al. 2022), while others analyzing data with similar structure have used independent and identically distributed (iid) random effects (Wu et al. 2020, Barry et al. 2022, Broen et al. 2023, Woodward et al. 2023, BurrIDGE et al. 2025). In the case of Wu et al. (2020), county-level latitude and longitude were additionally included as fixed-effect predictors to evaluate whether residual spatial correlation may have influenced the findings, acknowledging that unmodeled spatial structure could be a concern in this setting. In none of these cases was the choice formally justified, and to our knowledge no general guidance exists to inform this decision.

Despite these inconsistencies, a few prior studies have suggested that spatial structure becomes less consequential for accurate statistical inference in multilevel settings as within-area sample size increases. Savitz and Raudenbush (2009) noted that spatial borrowing is most beneficial when local sample sizes are small and that estimators based on no pooling, iid random effects, and spatially structured random effects converge as within-area sample size grows. Xu (2014) and Dasgupta et al. (2014) empirically observed that spatial and nonspatial models produced similar fixed effect estimates in individual-level datasets, though neither identified the sample size as the mechanism driving convergence nor attempted a theoretical comparison. While these works observed or remarked upon the convergence phenomenon, a formal assessment remains absent.

In this work, we formally investigate how within-area sample size impacts the need for spatially correlated random effects when fitting multilevel models to areal data. Working in the Bayesian setting, we demonstrate that when within-area sample size is large, the impact of the spatial prior distribution on posterior inference for the fixed effect of interest is negligible, and a nonspatial

random effect yields nearly identical results. Using the Leroux CAR distribution as a representative prior (Leroux et al. 2000), we make three contributions. First, working in a Markov chain Monte Carlo (MCMC) model fitting setting, we derive the full conditional distribution of the regression coefficient under both models and show that the absolute relative difference in variances converges to zero at rate $O(m^{-1})$, where m is the within-area sample size. Second, we derive a closed-form bound giving the minimum within-area sample size needed before the two models yield effectively equivalent inferences, depending on interpretable quantities including the spatial correlation parameter, the variance ratio, and properties of the covariate. Because these quantities can often be proposed prior to model fitting, the bound may serve as a practical tool for study design. Third, we evaluate the bound through simulation and show that it accurately identifies the replication threshold across a range of settings. These findings will provide guidance to practitioners determining whether a more complex spatial model is warranted for their application.

Section 2 introduces the models and notation underlying the derivations in Section 3, where we show that marginalizing over the random effects isolates how m enters the posterior variance of the regression parameter, leading to the convergence result and sample size bound. Section 4 evaluates these results through simulation and Section 5 concludes with further discussion. All proposed methods are implemented in the R package `SpThreshold`, available at <https://github.com/ShuqiLinn/SpThreshold>.

2. Multilevel model for areal spatial data

We consider a linear regression model for repeatedly measured areal spatial data. Our primary objective is accurate statistical inference for the regression parameter β_1 defined in (1), learning the relationship between the predictor and the outcome while properly adjusting for correlation in the data. Specifically, let Y_{ij} denote the response for the j^{th} observation within spatial unit i , where $i = 1, \dots, n$ and $j = 1, \dots, m$. We assume balanced replication across units and derive results based on a single covariate, with extensions discussed in Section 5. The model is given as

$$Y_{ij} = \beta_0 + \beta_1 x_{ij} + \theta_i + \varepsilon_{ij}, \quad \varepsilon_{ij} \mid \sigma^2 \stackrel{\text{iid}}{\sim} \mathcal{N}(0, \sigma^2), \quad (1)$$

where β_0 is an intercept parameter; β_1 is the coefficient for covariate x_{ij} ; θ_i is the location-specific random effect shared by all observations in unit i which induces correlation among observations from the same spatial unit; and ε_{ij} is an observation-level residual error term.

In addition to the clustering correlation induced by θ_i , it is common to account for spatial correlation among these parameters by introducing a spatial model. CAR models are widely used for areal data in the Bayesian setting due to the computational convenience of their conditional

distributions, with several specifications available (Lee 2011). We consider the CAR distribution of Leroux et al. (2000) where conditionally

$$\theta_i | \boldsymbol{\theta}_{-i}, \tau^2, \rho \stackrel{\text{ind}}{\sim} \mathcal{N} \left(\frac{\rho \sum_{i'=1}^n w_{ii'} \theta_{i'}}{\rho \sum_{i'=1}^n w_{ii'} + (1-\rho)}, \frac{\tau^2}{\rho \sum_{i'=1}^n w_{ii'} + (1-\rho)} \right), \quad i = 1, \dots, n,$$

with $\boldsymbol{\theta}_{-i}^\top = (\theta_1, \dots, \theta_{i-1}, \theta_{i+1}, \dots, \theta_n)$. This model allows for the borrowing of information spatially by specifying that *a priori* spatial unit i 's random effect is normally distributed and centered at a weighted average of values from neighboring units, where $w_{ii'}$ is a binary indicator describing whether units i and i' are neighbors (e.g., share a common border or vertex). Unlike the intrinsic CAR model (Besag 1974), this version represents a proper prior distribution for the vector of random effect parameters due to the inclusion of $\rho \in [0, 1)$. This parameter defines the amount of spatial borrowing that occurs; when $\rho = 0$, $\theta_i | \tau^2 \stackrel{\text{iid}}{\sim} \mathcal{N}(0, \tau^2)$ and as ρ approaches one, the original intrinsic CAR model is obtained.

Jointly, $\boldsymbol{\theta}^\top = (\theta_1, \dots, \theta_n)$ has a multivariate Gaussian distribution such that

$$\boldsymbol{\theta} | \tau^2, \rho \sim \mathcal{N}_n(\mathbf{0}_n, \tau^2 Q(\rho)^{-1}), \quad Q(\rho) = \rho \mathbf{L} + (1-\rho) \mathbf{I}_n,$$

where $\mathbf{0}_n$ is an n -length column vector with each entry equal to zero; $\mathbf{L} = \text{diag}(w_1, \dots, w_n) - \mathbf{W}$ is the graph Laplacian with \mathbf{W} the $n \times n$ adjacency matrix with entries $w_{ii'}$, and $w_i = \sum_{i'=1}^n w_{ii'}$; and \mathbf{I}_n is the n by n identity matrix. This multivariate Gaussian form allows for a convenient description of the joint distribution of the outcome vector and facilitates marginalizing out the $\boldsymbol{\theta}$ parameters, which we leverage in Section 3 when exploring the connection between m and the need for spatial modeling.

In matrix form, the model from (1) can be written as

$$\mathbf{Y} = \beta_0 \mathbf{1}_{nm} + \beta_1 \mathbf{x} + \mathbf{Z}\boldsymbol{\theta} + \boldsymbol{\varepsilon},$$

where $\mathbf{Y}^\top = (\mathbf{Y}_1^\top, \dots, \mathbf{Y}_n^\top)$ and $\mathbf{Y}_i^\top = (Y_{i1}, \dots, Y_{im})$; $\mathbf{1}_{nm}$ is an nm -length vector with each entry equal to one; \mathbf{x} is a vector containing the x_{ij} covariates and is sorted in the same way as \mathbf{Y} ; $\mathbf{Z} = \mathbf{I}_n \otimes \mathbf{1}_m$ is a sparse binary matrix that maps each individual to their respective areal unit, where \otimes represents the Kronecker product; and $\boldsymbol{\varepsilon}$ is a vector containing the ε_{ij} parameters and is sorted in the same way as \mathbf{Y} .

To complete the Bayesian model specification, we assign prior distributions to each model parameter. We assign flat priors to the regression coefficients, $f(\beta_0), f(\beta_1) \propto 1$; inverse-gamma priors to the variance parameters, $\sigma^2, \tau^2 \stackrel{\text{iid}}{\sim} \text{IG}(a, b)$; and a uniform prior to the correlation parameter, $\rho \sim \text{Uniform}(0, 1)$.

In Section A of the Supplementary Material, we detail the full conditional distributions needed to fit the model in (1) using standard MCMC methods based on two versions of the likelihood function;

conditional on $\boldsymbol{\theta}$ and marginalizing over $\boldsymbol{\theta}$. The conditional version of the model is implemented in the newly developed `SpThreshold` R package, supporting both spatial and nonspatial random effects, as well as multiple covariates.

3. When to model spatial correlation?

Our primary goal is to understand how marginal posterior inference for β_1 under the model in (1) is impacted as the within-unit sample size m increases, and specifically how it compares to the nonspatial version of (1) where $\rho = 0$ (i.e., $\theta_i | \tau^2 \stackrel{\text{iid}}{\sim} \mathcal{N}(0, \tau^2)$). To explore these relationships, we work with the full conditional distribution for β_1 based on the likelihood function where $\boldsymbol{\theta}$ has been marginalized out.

3.1. Full conditional distribution for β_1

After integrating out $\boldsymbol{\theta}$ from the model in (1), the distribution of \mathbf{Y} is given as

$$\mathbf{Y} | \beta_0, \beta_1, \sigma^2, \tau^2, \rho \sim \mathcal{N}_{nm}(\beta_0 \mathbf{1}_{nm} + \beta_1 \mathbf{x}, \Omega), \quad \Omega = \tau^2 \mathbf{Z} \mathbf{Q}(\rho)^{-1} \mathbf{Z}^\top + \sigma^2 \mathbf{I}_{nm}, \quad (2)$$

where all terms have been previously described. Based on the data distribution in (2) and given the flat prior distributions on the regression coefficients, the full conditional distribution of β_1 is given as

$$\beta_1 | \mathbf{Y}, \beta_0, \sigma^2, \tau^2, \rho \sim \mathcal{N}(\sigma_{\beta_1}^2 \mathbf{x}^\top \Omega^{-1} (\mathbf{Y} - \beta_0 \mathbf{1}_{nm}), \sigma_{\beta_1}^2), \quad \sigma_{\beta_1}^2 = \frac{1}{\mathbf{x}^\top \Omega^{-1} \mathbf{x}},$$

with full derivation details given in Section A.1 of the Supplementary Material. We note that if β_0 , σ^2 , τ^2 , and ρ were known, this full conditional distribution represents the posterior distribution of β_1 . Further, the variance of this distribution, $\sigma_{\beta_1}^2$, is only a function of σ^2 , τ^2 , and ρ . Although this expression conditions on unknown parameters, it isolates how m enters the posterior variance formula. This dependence carries through directly to the marginal posterior, as the full conditional distribution of β_1 appears as a component of the integrand when marginalizing over the remaining model parameters. Therefore, investigating this full conditional distribution can provide key insights into the marginal posterior distribution of interest.

Because measures of uncertainty for model parameters are more generally impacted by spatial correlation than point estimates (Diggle and Ribeiro 2007), except in cases of spatial confounding (Hodges and Reich 2010), we compare $\sigma_{\beta_1}^2$ under the full spatial model in (1) (i.e., $\sigma_{\beta_1}^2(\rho)$) to the same quantity under the nonspatial model with $\rho = 0$ (i.e., $\sigma_{\beta_1}^2(0)$). Differences in these expressions directly quantify how the spatial prior affects posterior inference for β_1 and how this relationship changes as m increases.

To make the roles of m and the covariance parameters in this comparison explicit, we derive a reduced-form expression for $\sigma_{\beta_1}^2$ that avoids matrix calculations involving the quantities of interest. To this end, we begin by simplifying the expression for $Q(\rho) = \rho L + (1 - \rho) I_n$. Because L is a real and symmetric matrix due to the form of the neighborhood adjacency matrix W , we can apply the spectral decomposition such that $L = U\Lambda U^\top$, where $U = [\mathbf{u}_1, \dots, \mathbf{u}_n]$ is the $n \times n$ matrix of orthonormal eigenvectors such that $U^\top U = U U^\top = I_n$; and $\Lambda = \text{diag}(\lambda_1, \dots, \lambda_n)$ contains the eigenvalues of L , with $0 = \lambda_1 < \lambda_2 \leq \dots \leq \lambda_n$ since we assume that the spatial map is connected (i.e., every unit can be reached from every other unit via a sequence of neighboring units). Therefore, $Q(\rho) = U \text{diag}(\rho\lambda_1 + 1 - \rho, \dots, \rho\lambda_n + 1 - \rho) U^\top$ with corresponding inverse $Q(\rho)^{-1} = \sum_{i=1}^n \mathbf{u}_i \mathbf{u}_i^\top / (\rho\lambda_i + 1 - \rho)$. Substituting this expression into the definition of Ω from (2), the covariance matrix of the marginal distribution of \mathbf{Y} can be written as

$$\Omega = \tau^2 \sum_{i=1}^n \frac{\mathbf{Z} \mathbf{u}_i \mathbf{u}_i^\top \mathbf{Z}^\top}{\rho\lambda_i + 1 - \rho} + \sigma^2 I_{nm}. \quad (3)$$

Next, we invert Ω using the Woodbury matrix identity (Woodbury 1950, Harville 1997) by noting that Ω from (3) can be written more generally as $\sigma^2 I_{nm} + \mathbf{Z}^* C \mathbf{Z}^{*\top}$, where $\mathbf{Z}^* = \mathbf{Z} U$ and $C = \tau^2 \text{diag}\{1/(\rho\lambda_1 + 1 - \rho), \dots, 1/(\rho\lambda_n + 1 - \rho)\}$. Applying the Woodbury matrix identity,

$$\Omega^{-1} = \frac{1}{\sigma^2} I_{nm} - \frac{1}{\sigma^4} \mathbf{Z}^* \left(C^{-1} + \frac{\mathbf{Z}^{*\top} \mathbf{Z}^*}{\sigma^2} \right)^{-1} \mathbf{Z}^{*\top}.$$

Because every spatial unit has the same sample size m ,

$$\begin{aligned} \mathbf{Z}^{*\top} \mathbf{Z}^* &= U^\top (I_n^\top \otimes \mathbf{1}_m^\top) (I_n \otimes \mathbf{1}_m) U \\ &= U^\top \{ (I_n^\top I_n) \otimes (\mathbf{1}_m^\top \mathbf{1}_m) \} U \\ &= m I_n, \end{aligned}$$

such that the inverse simplifies to

$$\Omega^{-1} = \frac{1}{\sigma^2} I_{nm} - \frac{\tau^2}{\sigma^2} \sum_{i=1}^n \frac{\mathbf{Z} \mathbf{u}_i \mathbf{u}_i^\top \mathbf{Z}^\top}{\sigma^2 (\rho\lambda_i + 1 - \rho) + m\tau^2}.$$

Therefore, the precision of the full conditional distribution of β_1 under the spatial model can be written as

$$\sigma_{\beta_1}^{-2}(\rho) = \frac{\mathbf{x}^\top \mathbf{x}}{\sigma^2} - \frac{\tau^2}{\sigma^2} \sum_{i=1}^n \frac{(\mathbf{x}^\top \mathbf{Z} \mathbf{u}_i)^2}{\sigma^2 (\rho\lambda_i + 1 - \rho) + m\tau^2}. \quad (4)$$

We can further simplify the expression in (4) by expanding $\mathbf{x}^\top \mathbf{Z} \mathbf{u}_i$. We first note that $\mathbf{Z}^\top \mathbf{x} = (I_n^\top \otimes \mathbf{1}_m^\top) \mathbf{x} = m \bar{\mathbf{x}}$ where $\bar{\mathbf{x}}^\top = (\bar{x}_1, \dots, \bar{x}_n)$ and $\bar{x}_i = m^{-1} \sum_{j=1}^m x_{ij}$. Therefore, $\mathbf{x}^\top \mathbf{Z} \mathbf{u}_i = m \sum_{i'=1}^n \bar{x}_{i'} \cdot u_{ii'}$, where $u_{ii'}$ denotes the i' th entry of \mathbf{u}_i . Without loss of generality, we further assume that the covariate has been centered and standardized prior to analysis such that its mean is equal

to zero and its population standard deviation (i.e., dividing by nm instead of $nm - 1$) is equal to one such that $\mathbf{x}^\top \mathbf{x} = nm$. Substituting this information into (4) yields

$$\sigma_{\beta_1}^{-2}(\rho) = \frac{nm}{\sigma^2} - \frac{m^2\tau^2}{\sigma^2} \sum_{i=1}^n \frac{(\sum_{i'=1}^n \bar{x}_{i'} \cdot u_{ii'})^2}{\sigma^2(\rho\lambda_i + 1 - \rho) + m\tau^2}. \quad (5)$$

Similarly, we obtain the comparable precision expression under the nonspatial model by plugging in $\rho = 0$ into (5) such that

$$\sigma_{\beta_1}^{-2}(0) = \frac{nm}{\sigma^2} - \frac{m^2\tau^2}{\sigma^2(\sigma^2 + m\tau^2)} \sum_{i=1}^n \left(\sum_{i'=1}^n \bar{x}_{i'} \cdot u_{ii'} \right)^2. \quad (6)$$

These expressions are useful in this setting as they are functions of quantities that are available from the raw data (i.e., sample sizes, covariate values, and eigenvectors/eigenvalues based on the spatial adjacency matrix) and the covariance parameters. To empirically validate the findings in (5) and (6), we compare them directly to the matrix algebra versions given by $1/(\mathbf{x}^\top \Omega^{-1} \mathbf{x})$ by randomly sampling different spatial adjacency matrices, covariate values, and parameter values, and computing both forms. Results were in agreement across all simulations, and code for this empirical analysis can be found in the `paper/` subdirectory of the `SpThreshold` repository.

3.2. Within-area sample size threshold

To determine how posterior inference for β_1 differs between the spatial and nonspatial models as m increases, we analyze the absolute relative difference in variances of the full conditional distributions,

$$\left| \frac{\sigma_{\beta_1}^2(\rho) - \sigma_{\beta_1}^2(0)}{\sigma_{\beta_1}^2(0)} \right| = \left| \frac{\sigma_{\beta_1}^{-2}(0) - \sigma_{\beta_1}^{-2}(\rho)}{\sigma_{\beta_1}^{-2}(\rho)} \right|, \quad (7)$$

using the results from (5) and (6). We show that this quantity converges to zero at a rate $O(m^{-1})$ and derive a closed-form sample size threshold m^* to bound the difference within a desired level of error.

To simplify notation, from (5) and (6) we define $d_i \equiv (\sum_{i'=1}^n \bar{x}_{i'} \cdot u_{ii'})^2$ and $d. \equiv \sum_{i=1}^n d_i$. The numerator in (7) can then be written as

$$\frac{m^2\tau^2}{\sigma^2} \left[\left\{ \sum_{i=1}^n \frac{d_i}{\sigma^2(\rho\lambda_i + 1 - \rho) + m\tau^2} \right\} - \frac{d.}{\sigma^2 + m\tau^2} \right].$$

To bound this expression, we apply the expansion $(1 + g)^{-1} = 1 - g + O(g^2)$ for small g giving

$$\begin{aligned} \{\sigma^2(\rho\lambda_i + 1 - \rho) + m\tau^2\}^{-1} &= \frac{1}{m\tau^2} \left\{ 1 + \frac{\sigma^2(\rho\lambda_i + 1 - \rho)}{m\tau^2} \right\}^{-1} \\ &= \frac{1}{m\tau^2} \left\{ 1 - \frac{\sigma^2(\rho\lambda_i + 1 - \rho)}{m\tau^2} + O(m^{-2}) \right\} \end{aligned}$$

$$= \frac{1}{m\tau^2} \left\{ 1 - \frac{\sigma^2(\rho\lambda_i + 1 - \rho)}{m\tau^2} \right\} + O(m^{-3}).$$

Similarly, with $\rho = 0$, $(\sigma^2 + m\tau^2)^{-1} = \frac{1}{m\tau^2} \left(1 - \frac{\sigma^2}{m\tau^2} \right) + O(m^{-3})$. Plugging these results back into (5) and (6), we obtain

$$\begin{aligned} \sigma_{\beta_1}^{-2}(\rho) &= \frac{nm}{\sigma^2} - \frac{m^2\tau^2}{\sigma^2} \left[\sum_{i=1}^n \frac{d_i}{m\tau^2} \left\{ 1 - \frac{\sigma^2(\rho\lambda_i + 1 - \rho)}{m\tau^2} \right\} + O(m^{-3}) \right] \\ &= \frac{nm}{\sigma^2} - \frac{md.}{\sigma^2} + \sum_{i=1}^n \frac{d_i}{\tau^2} (\rho\lambda_i + 1 - \rho) + O(m^{-1}) \\ &= \frac{nm}{\sigma^2} - \frac{md.}{\sigma^2} + \frac{d.}{\tau^2} + \frac{\rho}{\tau^2} \sum_{i=1}^n d_i (\lambda_i - 1) + O(m^{-1}) \end{aligned}$$

and $\sigma_{\beta_1}^{-2}(0) = \frac{nm}{\sigma^2} - \frac{md.}{\sigma^2} + \frac{d.}{\tau^2} + O(m^{-1})$. Therefore, the numerator in (7) can be further simplified as $\frac{\rho}{\tau^2} \sum_{i=1}^n d_i (1 - \lambda_i) + O(m^{-1})$.

The denominator of (7) can also be simplified such that $\sigma_{\beta_1}^{-2}(\rho) = \frac{m(n-d.)}{\sigma^2} \{1 + O(m^{-1})\}$, resulting in an absolute difference of

$$\frac{\frac{\rho}{\tau^2} \sum_{i=1}^n d_i (1 - \lambda_i) + O(m^{-1})}{\frac{m(n-d.)}{\sigma^2} \{1 + O(m^{-1})\}} = \left\{ \frac{\rho\sigma^2}{\tau^2 m(n-d.)} \sum_{i=1}^n d_i (1 - \lambda_i) + O(m^{-2}) \right\} \{1 + O(m^{-1})\}, \quad (8)$$

where the previous expansion was again applied to the denominator term. Expression (8) reduces to $\{O(m^{-1}) + O(m^{-2})\} \{1 + O(m^{-1})\} = O(m^{-1})$, confirming that the absolute relative difference in (7) is $O(m^{-1})$.

Further, using the form in (8), the leading-order term of the absolute relative difference is $\left| \frac{\rho\sigma^2}{\tau^2 m(n-d.)} \sum_{i=1}^n d_i (1 - \lambda_i) \right|$. Setting a tolerance γ for the maximum acceptable error and solving for m , we obtain the within-area sample size threshold

$$m^* \geq \max \left\{ 2, \left\lceil \frac{\sigma^2 \rho \sum_{i=1}^n d_i (1 - \lambda_i)}{\gamma \tau^2 (n - \sum_{i=1}^n \bar{x}_i^2)} \right\rceil \right\}, \quad (9)$$

where we set a lower bound of 2 given that it is the smallest possible sample size such that we are still working with multilevel data, and note that $d. = \|\mathbf{U}^\top \bar{\mathbf{x}}\|^2 = \|\bar{\mathbf{x}}\|^2 = \sum_{i=1}^n \bar{x}_i^2$ since \mathbf{U} is orthonormal. The threshold in (9) is a function of three interpretable quantities: the spatial correlation parameter ρ , the variance ratio $\kappa = \tau^2/\sigma^2$ (which enters the numerator as $1/\kappa$), and the covariate structure through the projections d_i . Stronger spatial correlation or smaller variance ratio requires more replication before spatial smoothing becomes negligible, as both make the spatial prior more influential.

The projections $d_i = (\sum_{i'=1}^n \bar{x}_{i'} \cdot \mathbf{u}_{ii'})^2$ decompose the between-location covariate variation across the eigenvectors of the graph Laplacian, which represent spatial patterns at progressively finer scales: \mathbf{u}_1 corresponds to a constant (global mean), \mathbf{u}_2 to the smoothest nontrivial contrast, and

successive eigenvectors to increasingly localized variation. When covariate means vary little across locations, the d_i are uniformly small and the threshold is low. When they exhibit smooth spatial trends aligned with the leading eigenvectors, the d_i concentrate on the components where the two models differ most, and a larger m is needed.

4. Simulation study

We design a simulation study to evaluate the theoretical results of Section 3. We have two primary objectives: first, to examine how the differences in the marginal posterior variance and mean of β_1 between the spatial and nonspatial models change as within-area sample size m increases, and second, to assess how well the asymptotic bound m^* identifies the replication level at which the two models yield effectively equivalent inference. We explore both objectives across varying levels of spatial correlation, signal-to-noise ratio, and covariate structure.

4.1. Study design

We simulate data from (1) with $n \in \{25, 100, 400\}$ spatial units. For a selected n , we first simulate a random connected spatial map with n units to define the adjacency matrix W . Summary statistics of the resulting graphs and example realizations are provided in Section C of the Supplementary Material. Next, we generate spatial random effects $\theta \mid \tau^2, \rho \sim \mathcal{N}_n(\mathbf{0}_n, \tau^2 Q(\rho)^{-1})$ while varying spatial correlation $\rho \in \{0.05, 0.50, 0.95\}$ and variance ratio $\kappa = \tau^2/\sigma^2 \in \left\{\frac{0.05}{0.95}, \frac{0.50}{0.50}, \frac{0.95}{0.05}\right\}$, where $\tau^2 + \sigma^2 = 1$ so that the total marginal variance is held constant. Small values of κ correspond to settings where spatial random effects contribute little relative to observation-level noise, while large κ indicates that most variability is attributable to location-level differences. Finally, we sample $\beta_0, \beta_1 \stackrel{\text{iid}}{\sim} \mathcal{N}(0, 1)$.

We also consider three different covariate structure settings (C1-C3). In C1, $x_{ij} \stackrel{\text{iid}}{\sim} \mathcal{N}(0, 1)$ for all i and j , so covariate variation is entirely within locations. The \bar{x}_i are approximately zero resulting in small d_i and m^* , so we expect spatial and nonspatial inference to be similar even at small m . In C2, $x_{ij} \mid \mu_i \stackrel{\text{iid}}{\sim} \mathcal{N}(\mu_i, 1)$ with location-specific means $\mu_i \stackrel{\text{iid}}{\sim} \mathcal{N}(0, 1)$, introducing between-location variation. In this case, m^* may be larger as the \bar{x}_i are not all approximately equal to zero. In C3, $x_{ij} = \mu_i$ with $\mu_i \stackrel{\text{iid}}{\sim} \mathcal{N}(0, 1)$, so the covariate is entirely a location-level attribute. Under such covariate structure, $x_{ij} = \bar{x}_i$, and $\sum_{j=1}^m x_{ij}^2 = m\bar{x}_i^2$ for every i . Combined with the population standardization that gives $\sum_{i=1}^n \sum_{j=1}^m x_{ij}^2 = nm$, this suggests $\sum_{i=1}^n \bar{x}_i^2 = n$ and therefore, the denominator in (9) is exactly zero. Hence, m^* is infinite and we expect the two models to remain distinguishable at any finite m .

Within-area replication sample sizes range over $m \in \{1, 2, 5, 10, 20, 50, 80, 100, 200\}$. For each combination of (n, m, ρ, κ) and covariate structure setting (in total 729 unique settings), we generate 100 independent datasets for analysis. A summary of all simulation settings is provided in Table 1.

To illustrate the range of spatial structures implied by these settings, Figure 1 displays example realizations of θ across all combinations of ρ and κ on a 10×10 grid where spatial neighbors are defined based on shared borders and vertices. Increasing ρ produces smoother spatial patterns, while increasing κ amplifies the magnitude of the spatial random effects.

Table 1 Summary of simulation study settings.

Parameter	Values
Datasets per setting	100
Spatial units (n)	25, 100, 400
Spatial correlation (ρ)	0.05, 0.50, 0.95
Variance ratio ($\kappa = \tau^2/\sigma^2$)	0.05/0.95, 0.50/0.50, 0.95/0.05
Within-area replication (m)	1, 2, 5, 10, 20, 50, 80, 100, 200
Covariate structure	C1: $x_{ij} \stackrel{\text{iid}}{\sim} \mathcal{N}(0, 1)$, C2: $x_{ij} \mid \mu_i \stackrel{\text{iid}}{\sim} \mathcal{N}(\mu_i, 1)$; $\mu_i \stackrel{\text{iid}}{\sim} \mathcal{N}(0, 1)$, C3: $x_{ij} = \mu_i$; $\mu_i \stackrel{\text{iid}}{\sim} \mathcal{N}(0, 1)$

For each dataset, we fit both models using the MCMC algorithm that directly includes θ as part of the parameter space. This algorithm is detailed in Section A of the Supplementary Material and implemented in the `SpThreshold` R package. Prior distributions are given in Section 2, with inverse-gamma hyperparameters $a = b = 0.01$ to induce weakly informative priors on σ^2 and τ^2 . Without loss of generality, we center and standardize the covariate to have mean zero and population variance one prior to analysis.

When updating ρ using the Metropolis algorithm, the proposal distribution standard deviation is adapted during the burn-in period using the Robbins-Monro scheme of Roberts and Rosenthal (2009), targeting an acceptance rate of 0.234 (Gelman et al. 1997) and held fixed thereafter. The nonspatial model is fit using a Gibbs sampler with all updates drawn directly from closed-form full conditional distributions. For both models we collect 75,000 iterations, discard the first 15,000 as burn-in, and thin by a factor of 5, yielding 12,000 posterior draws. Convergence was assessed by visual inspection of trace plots across a subset of analyses. From these posterior samples we compute the posterior mean and variance of β_1 under each model, and record the absolute differences in posterior means and the absolute relative difference in posterior variances between the two models. Results are averaged across the 100 datasets from each setting.

4.2. Results

Figure 2 displays the absolute relative difference in the marginal posterior variance of β_1 between the spatial (i.e., $\text{Var}(\beta_1 | \mathbf{Y}, \rho)$) and nonspatial (i.e., $\text{Var}(\beta_1 | \mathbf{Y}, 0)$) models, averaged over 100 simulations, as a function of the within-area replication m , for $n = 100$ spatial units. Results for $n = 25$

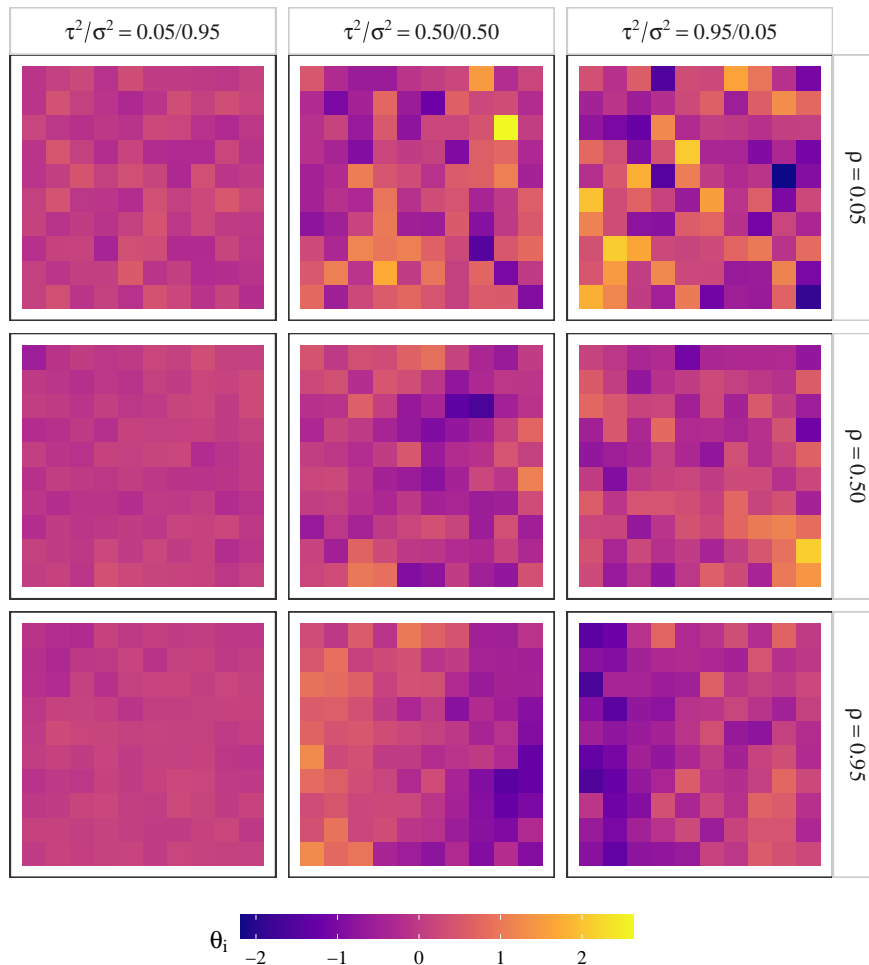


Figure 1 Example realizations of the spatial random effects θ across different levels of spatial correlation ρ and variance ratio $\kappa = \tau^2/\sigma^2$, generated on a 10×10 queen adjacency grid for illustration. The actual simulation study uses random connected graphs as described in the main text.

and $n = 400$ are shown in Figures B.1–B.4 of the Supplementary Materials. The three covariate structure settings are shown in each panel, with the dashed red line indicating tolerance $\gamma = 0.05$. Because $m^* \approx 2$ on average under C1 and is infinite under C3, we plot the asymptotic bound only under C2, shown as the dashed blue vertical line.

In C1, where all covariate variation is within locations, the absolute relative difference in variances is near or below γ across all settings, consistent with the theoretical prediction that small d_i values yield a small bound. When between-location variation is introduced (C2), the difference is larger at small m but decreases steadily as m grows, crossing below γ near the value predicted by m^* in all nine panels. The bound is most demanding when ρ is large and κ is small (bottom-left panel, $m^* = 482$), where strong spatial correlation and weak signal make the spatial prior most influential; conversely, when κ is large (right column), the within-area likelihood dominates even at small m

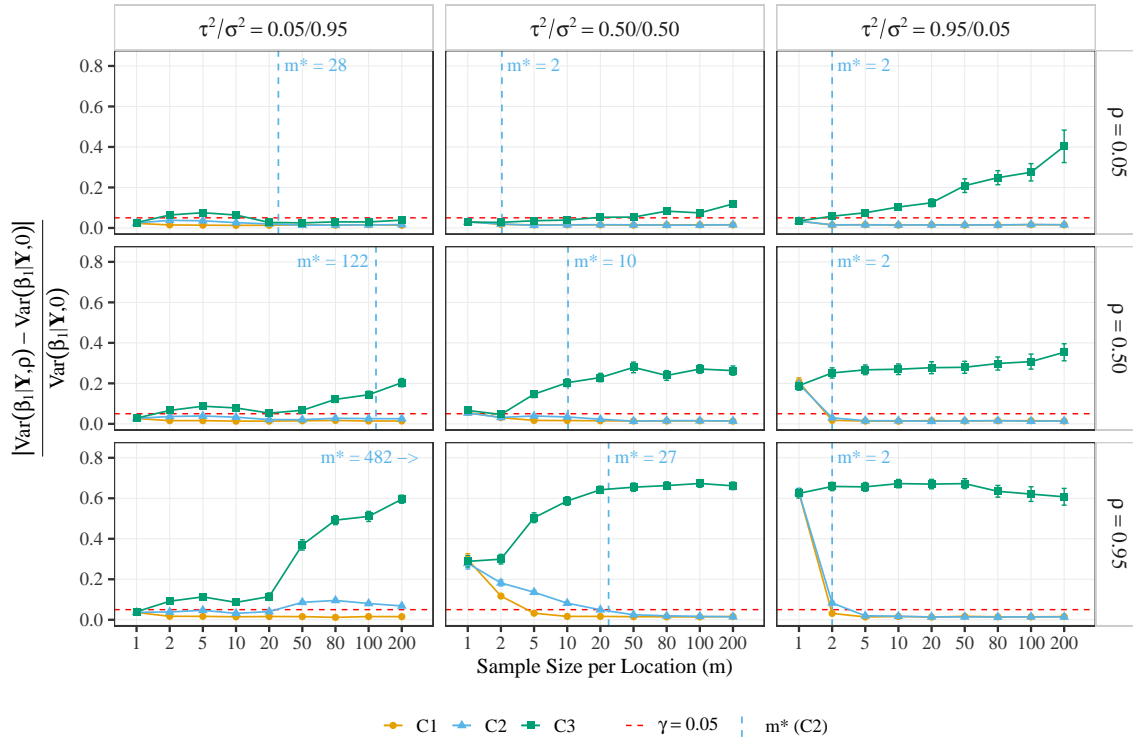


Figure 2 Absolute relative difference in the marginal posterior variance of β_1 between the spatial (i.e., $\text{Var}(\beta_1|\mathbf{Y}, \rho)$) and nonspatial (i.e., $\text{Var}(\beta_1|\mathbf{Y}, 0)$) models, averaged over 100 datasets, for $n = 100$ spatial units. Columns correspond to the variance ratio $\kappa = \tau^2/\sigma^2$ and rows to the spatial correlation ρ . The three curves represent the three covariate structures, C1-C3, described in Table 1. The dashed red horizontal line marks the tolerance $\gamma = 0.05$; the dashed blue vertical line marks the asymptotic bound m^* computed under C2. Error bars are pointwise 95% Monte Carlo confidence intervals across datasets.

and the bound reduces to $m^* = 2$. Under C3, the absolute relative variance difference remains well above γ throughout the range of m considered, indicating that a spatial model remains necessary when the covariate is entirely a location-level attribute.

Figure 3 shows the absolute difference in posterior means of β_1 between the two models, averaged over 100 simulations. Under C1 and C2, the averaged difference is close to zero across all settings. In C3, the discrepancy is larger and does not diminish as m increases, particularly at high ρ and κ . When the covariate has no within-location variation, it is confounded with the spatial random effects, and the two models yield different point estimates.

5. Discussion

In this work, we investigated the role of within-area sample size in determining when spatial and nonspatial models yield equivalent inference on regression coefficients in a multilevel model for areal data. Working within a hierarchical Bayesian framework using the Leroux CAR prior, we

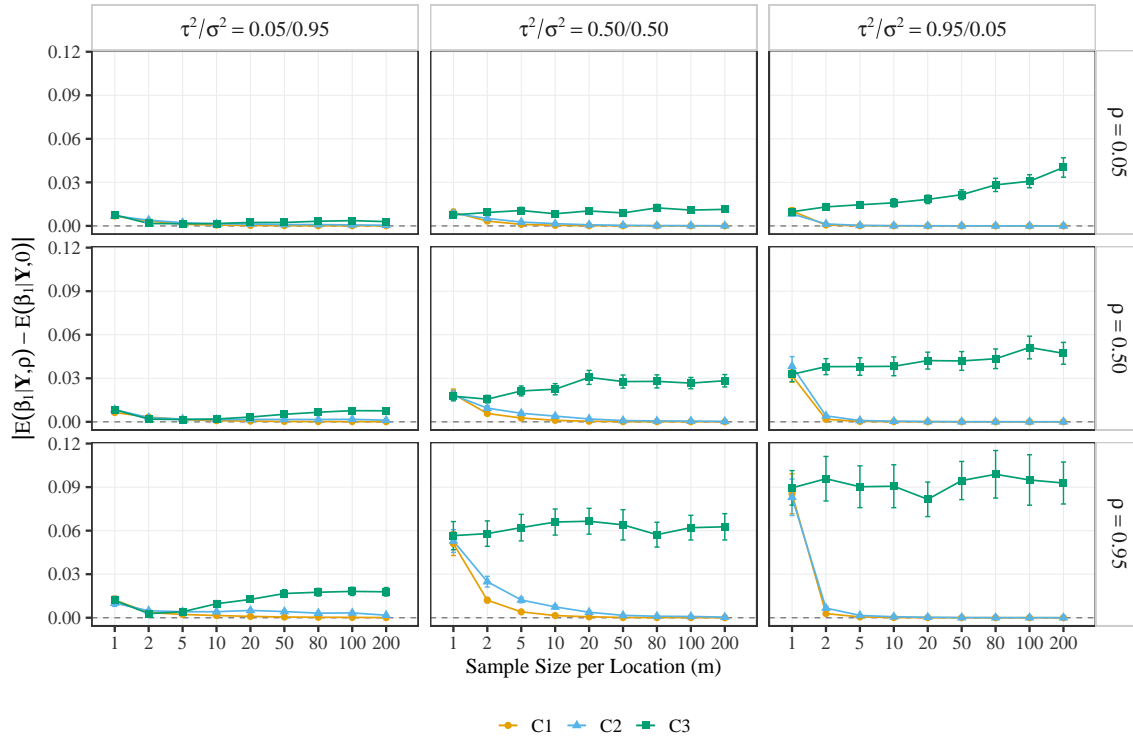


Figure 3 Absolute difference in the marginal posterior mean of β_1 between the spatial (i.e., $E(\beta_1|\mathbf{Y}, \rho)$) and nonspatial (i.e., $E(\beta_1|\mathbf{Y}, 0)$) models, averaged over 100 datasets, for $n = 100$ spatial units. Columns correspond to the variance ratio $\kappa = \tau^2/\sigma^2$ and rows to the spatial correlation ρ . The three curves represent the three covariate structure settings, C1-C3, described in Table 1. Error bars are pointwise 95% Monte Carlo confidence intervals across datasets.

derived the full conditional distribution of a regression coefficient under both specifications and showed that the absolute relative difference in marginal posterior variances converges to zero at rate $O(m^{-1})$. We further derived a closed-form sample size threshold m^* depending on the spatial correlation parameter ρ , the variance ratio $\kappa = \frac{\tau^2}{\sigma^2}$, and the alignment between the covariate and the spatial structure of the data, and showed through simulation that it accurately identifies the replication level beyond which the two models produce effectively indistinguishable inference.

Importantly, the covariate's role operates through the projections d_i , which measure how strongly the location-level covariate means align with the eigenvectors of the graph Laplacian. Covariates that track smooth spatial gradients, concentrating on the leading eigenvectors where the spatial and nonspatial models differ most, require substantially more replication before spatial modeling becomes unnecessary, while covariates that vary in an unstructured way across locations demand much less. When the covariate has no within-location variation at all, this alignment is total and m^* is infinite, meaning spatial modeling remains necessary regardless of replication.

These results have practical implications for both study design and analysis. Investigators working with spatially referenced areal data who have access to multiple observations per spatial unit can evaluate m^* before fitting a full spatial model to determine whether the added complexity is warranted. Because the bound depends on quantities that can be estimated from a pilot analysis or from existing knowledge about the study setting, this assessment can be carried out at the design stage. When the available replication exceeds m^* , a simpler nonspatial hierarchical model may be used without materially affecting inference on regression coefficients, avoiding the computational burden of spatial MCMC algorithms. We note that this guidance applies specifically to inference on regression coefficients; if the goal is spatial prediction (i.e., inferring outcomes at unobserved or sparsely observed locations, where information must be borrowed from neighbors rather than drawn from within-area replication), spatial structure remains important regardless of replication. Both versions of the model can be fit using the `SpThreshold` R package. Although we derived results for a single covariate, the threshold m^* applies directly in the multiple covariate setting, as the full conditional distribution variance of any regression coefficient depends only on the corresponding covariate vector and the covariance parameters, with all other predictors absorbed into the conditioning set.

Several extensions could broaden the framework’s applicability. Throughout this work, we assumed balanced replication across spatial units, which enabled a clean closed-form expression for the posterior variance. In practice, replication often varies across areas. The current bound can be applied conservatively by using the minimum within-area sample size across all locations. Developing an area-specific threshold that accounts for heterogeneous sample sizes would be useful for applications where some areas are data-rich and others sparse, though the additional complexity may limit interpretability.

Areal data often take the form of counts modeled using Poisson, negative binomial, or binomial likelihoods rather than Gaussian outcomes, and deriving analogous results for these settings is a natural next step. While auxiliary variable approaches exist for some of these likelihoods that yield conjugacy under carefully chosen priors (Held and Holmes 2006, Polson et al. 2013), the auxiliary variables themselves are often conditioned on in the derivations, making a useful closed-form solution difficult to obtain. Additionally, spatio-temporal extensions, where replication arises across both space and time and the model parameters may vary temporally, are another important direction given the increasing availability of longitudinal spatially referenced datasets.

Overall, our findings suggest that for inference on regression coefficients, the practical value of spatial modeling in multilevel areal data depends critically on two factors: the within-area sample size and the structure of the covariate. When the covariate varies within locations, sufficient replication allows a nonspatial hierarchical model to yield effectively equivalent inference while

avoiding the overhead of spatial modeling. As individual-level spatially referenced data become increasingly available across the health, environmental, and social sciences, the question of when spatial structure is necessary will only grow in relevance, and these results provide a useful starting point for understanding the major drivers of this decision.

References

- Asare EO, Warren JL, Pitzer VE (2022) Spatiotemporal patterns of diarrhea incidence in Ghana and the impact of meteorological and socio-demographic factors. *Frontiers in Epidemiology* 2:871232.
- Banerjee S, Carlin BP, Gelfand AE (2003) *Hierarchical modeling and analysis for spatial data* (Chapman and Hall/CRC).
- Barry Y, Le Strat Y, Azria E, Gorza M, Pilkington H, Vandentorren S, et al. (2022) Ability of municipality-level deprivation indices to capture social inequalities in perinatal health in France: A nationwide study using preterm birth and small for gestational age to illustrate their relevance. *BMC Public Health* 22(1):919.
- Besag J (1974) Spatial interaction and the statistical analysis of lattice systems. *Journal of the Royal Statistical Society: Series B (Methodological)* 36(2):192–225.
- Besag J, York J, Mollié A (1991) Bayesian image restoration, with two applications in spatial statistics. *Annals of the Institute of Statistical Mathematics* 43(1):1–20.
- Bravo MA, Warren JL, Leong MC, Deziel NC, Kimbro RT, Bell ML, et al. (2022) Where is air quality improving, and who benefits? a study of PM_{2.5} and ozone over 15 years. *American Journal of Epidemiology* 191(7):1258–1269.
- Broen K, Dickens J, Trangucci R, Ogwang MD, Tenge CN, Masalu N, et al. (2023) Burkitt lymphoma risk shows geographic and temporal associations with Plasmodium falciparum infections in Uganda, Tanzania, and Kenya. *Proceedings of the National Academy of Sciences* 120(2):e2211055120.
- Burridge JV, Baer RJ, Chambers CD (2025) Association between census-tract social vulnerability index and preterm birth rates. *Pregnancy* 1(6):e70142.
- Cars BS, Northrup JM, Beasley K, Beasley P, Beasley K, Shafer AB (2025) Environmental and temporal factors affecting record white-tailed deer antler characteristics in Ontario, Canada. *The Journal of Wildlife Management* 90(4):e70191.
- Choi YG, Hanrahan LP, Norton D, Zhao YQ (2022) Simultaneous spatial smoothing and outlier detection using penalized regression, with application to childhood obesity surveillance from electronic health records. *Biometrics* 78(1):324–336.
- Clark CJ, Warren JL, Kadan-Lottick N, Ma X, Bell ML, Saiers JE, et al. (2021) Community concern and government response: Identifying socio-economic and demographic predictors of oil and gas complaints and drinking water impairments in Pennsylvania. *Energy Research & Social Science* 76:102070.

- Cressie N (2015) *Statistics for Spatial Data* (John Wiley & Sons).
- Dasgupta P, Cramb SM, Aitken JF, Turrell G, Baade PD (2014) Comparing multilevel and bayesian spatial random effects survival models to assess geographical inequalities in colorectal cancer survival: a case study. *International Journal of Health Geographics* 13(1):36.
- Diggle PJ, Ribeiro PJ (2007) *Classical Parameter Estimation*, 99–133. Springer Series in Statistics (Springer New York), ISBN 978-0-387-48536-2.
- Djeudeu D, Moebus S, Ickstadt K (2022) Multilevel conditional autoregressive models for longitudinal and spatially referenced epidemiological data. *Spatial and Spatio-temporal Epidemiology* 41:100477.
- Dong G, Ma J, Harris R, Pryce G (2016) Spatial random slope multilevel modeling using multivariate conditional autoregressive models: A case study of subjective travel satisfaction in beijing. *Annals of the American Association of Geographers* 106(1):19–35.
- Dormann CF, McPherson JM, Araújo MB, Bivand R, Bolliger J, Carl G, et al. (2007) Methods to account for spatial autocorrelation in the analysis of species distributional data: a review. *Ecography* 30(5):609–628.
- Gamerman D, Lopes HF (2006) *Markov Chain Monte Carlo: Stochastic Simulation for Bayesian Inference* (Chapman and Hall/CRC), 2nd edition.
- Gelfand AE, Smith AF (1990) Sampling-based approaches to calculating marginal densities. *Journal of the American Statistical Association* 85(410):398–409.
- Gelman A, Gilks WR, Roberts GO (1997) Weak convergence and optimal scaling of random walk metropolis algorithms. *Annals of Applied Probability* 7(1):110–120.
- Geman S, Geman D (1984) Stochastic relaxation, gibbs distributions, and the bayesian restoration of images. *IEEE Transactions on Pattern Analysis and Machine Intelligence* PAMI-6(6):721–741.
- Harville DA (1997) *Matrix algebra from a statistician's perspective* (Springer).
- Held L, Holmes CC (2006) Bayesian auxiliary variable models for binary and multinomial regression. *Bayesian Analysis* 1(1):145–168.
- Hodges JS, Reich BJ (2010) Adding spatially-correlated errors can mess up the fixed effect you love. *The American Statistician* 64(4):325–334.
- Lee D (2011) A comparison of conditional autoregressive models used in bayesian disease mapping. *Spatial and Spatio-temporal Epidemiology* 2(2):79–89.
- Legendre P (1993) Spatial autocorrelation: trouble or new paradigm? *Ecology* 74(6):1659–1673.
- Leroux BG, Lei X, Breslow N (2000) Estimation of disease rates in small areas: A new mixed model for spatial dependence. Halloran ME, Berry D, eds., *Statistical Models in Epidemiology, the Environment, and Clinical Trials*, volume 116 of *The IMA Volumes in Mathematics and its Applications*, 179–191 (Springer), ISBN 978-1-4612-1284-3.

- Li J, Murray-Watson RE, St Cyr SB, Grad YH, Warren JL, Yaesoubi R (2025) Association between city-level sociodemographic and health factors and the prevalence of antimicrobial-resistant gonorrhoea in the us, 2000–2019: a spatial–temporal modeling study. *The Lancet Regional Health–Americas* 43:101006.
- Metropolis N, Rosenbluth AW, Rosenbluth MN, Teller AH, Teller E (1953) Equation of state calculations by fast computing machines. *The Journal of Chemical Physics* 21(6):1087–1092.
- Polson NG, Scott JG, Windle J (2013) Bayesian inference for logistic models using pólya–gamma latent variables. *Journal of the American Statistical Association* 108(504):1339–1349.
- Roberts GO, Rosenthal JS (2009) Examples of adaptive MCMC. *Journal of Computational and Graphical Statistics* 18(2):349–367.
- Savitz NV, Raudenbush SW (2009) Exploiting spatial dependence to improve measurement of neighborhood social processes. *Sociological Methodology* 39(1):151–183.
- Woodbury MA (1950) *Inverting modified matrices* (Department of Statistics, Princeton University).
- Woodward SM, Mork D, Wu X, Hou Z, Braun D, Dominici F (2023) Combining aggregate and individual-level data to estimate individual-level associations between air pollution and covid-19 mortality in the united states. *PLOS Global Public Health* 3(8):e0002178.
- Wu X, Nethery RC, Sabath MB, Braun D, Dominici F (2020) Air pollution and covid-19 mortality in the united states: Strengths and limitations of an ecological regression analysis. *Science Advances* 6(45):eabd4049.
- Xu H (2014) Comparing spatial and multilevel regression models for binary outcomes in neighborhood studies. *Sociological Methodology* 44(1):229–272.

Appendix A: Full conditional distributions

In this section, we provide derivation details for the full conditional distributions used to fit the model from the main text via Markov chain Monte Carlo (MCMC) sampling (Metropolis et al. 1953, Geman and Geman 1984, Gelfand and Smith 1990). Derivations are based on the conditional likelihood (i.e., treating $\boldsymbol{\theta}$ as part of the parameter space), which is the version used to fit both the spatial and nonspatial models in the simulation study in Section 4 of the main text. We additionally derive the full conditional distribution for $\boldsymbol{\beta}$ based on the marginal likelihood (i.e., after integrating $\boldsymbol{\theta}$ out), which is the starting point for the derivations in Section 3 of the main text.

A.1. Regression coefficients $\boldsymbol{\beta}$

Under the conditional likelihood, let $\mathbf{r} = \mathbf{Y} - \mathbf{Z}\boldsymbol{\theta}$. Because $f(\boldsymbol{\beta}) \propto 1$, the full conditional distribution of $\boldsymbol{\beta}$ is proportional to the likelihood contribution from the observed data,

$$\begin{aligned} f(\boldsymbol{\beta} | \text{rest}) &\propto \exp \left\{ -\frac{1}{2\sigma^2} (\mathbf{r} - \mathbf{X}\boldsymbol{\beta})^\top (\mathbf{r} - \mathbf{X}\boldsymbol{\beta}) \right\} \\ &\propto \exp \left\{ -\frac{1}{2\sigma^2} (\boldsymbol{\beta}^\top \mathbf{X}^\top \mathbf{X} \boldsymbol{\beta} - 2\boldsymbol{\beta}^\top \mathbf{X}^\top \mathbf{r}) \right\} \\ &= \exp \left\{ -\frac{1}{2} (\boldsymbol{\beta} - \hat{\boldsymbol{\beta}})^\top \frac{\mathbf{X}^\top \mathbf{X}}{\sigma^2} (\boldsymbol{\beta} - \hat{\boldsymbol{\beta}}) \right\}, \end{aligned}$$

where $\hat{\boldsymbol{\beta}} = (\mathbf{X}^\top \mathbf{X})^{-1} \mathbf{X}^\top \mathbf{r}$. Therefore,

$$\boldsymbol{\beta} | \text{rest} \sim \mathcal{N}_2 \left((\mathbf{X}^\top \mathbf{X})^{-1} \mathbf{X}^\top (\mathbf{Y} - \mathbf{Z}\boldsymbol{\theta}), \sigma^2 (\mathbf{X}^\top \mathbf{X})^{-1} \right).$$

After integrating $\boldsymbol{\theta}$ out of the model, the marginal likelihood is $\mathbf{Y} | \boldsymbol{\beta}, \sigma^2, \tau^2, \rho \sim \mathcal{N}_{nm}(\mathbf{X}\boldsymbol{\beta}, \Omega)$, where $\Omega = \tau^2 \mathbf{Z} \mathbf{Q}(\rho)^{-1} \mathbf{Z}^\top + \sigma^2 \mathbf{I}_{nm}$. The full conditional distribution of $\boldsymbol{\beta}$ satisfies

$$\begin{aligned} f(\boldsymbol{\beta} | \text{rest}) &\propto \exp \left\{ -\frac{1}{2} (\mathbf{Y} - \mathbf{X}\boldsymbol{\beta})^\top \Omega^{-1} (\mathbf{Y} - \mathbf{X}\boldsymbol{\beta}) \right\} \\ &\propto \exp \left\{ -\frac{1}{2} (\boldsymbol{\beta}^\top \mathbf{X}^\top \Omega^{-1} \mathbf{X} \boldsymbol{\beta} - 2\boldsymbol{\beta}^\top \mathbf{X}^\top \Omega^{-1} \mathbf{Y}) \right\} \\ &= \exp \left\{ -\frac{1}{2} (\boldsymbol{\beta} - \tilde{\boldsymbol{\beta}})^\top \mathbf{X}^\top \Omega^{-1} \mathbf{X} (\boldsymbol{\beta} - \tilde{\boldsymbol{\beta}}) \right\}, \end{aligned}$$

where $\tilde{\boldsymbol{\beta}} = (\mathbf{X}^\top \Omega^{-1} \mathbf{X})^{-1} \mathbf{X}^\top \Omega^{-1} \mathbf{Y}$. Therefore,

$$\boldsymbol{\beta} | \text{rest} \sim \mathcal{N}_2 \left((\mathbf{X}^\top \Omega^{-1} \mathbf{X})^{-1} \mathbf{X}^\top \Omega^{-1} \mathbf{Y}, (\mathbf{X}^\top \Omega^{-1} \mathbf{X})^{-1} \right).$$

In particular, the full conditional of β_1 conditional on β_0 is

$$\beta_1 | \mathbf{Y}, \beta_0, \sigma^2, \tau^2, \rho \sim \mathcal{N}(\mu_{\beta_1}, \sigma_{\beta_1}^2),$$

where

$$\sigma_{\beta_1}^2 = \frac{1}{\mathbf{x}^\top \Omega^{-1} \mathbf{x}}, \quad \mu_{\beta_1} = \sigma_{\beta_1}^2 \mathbf{x}^\top \Omega^{-1} (\mathbf{Y} - \beta_0 \mathbf{1}_{nm}).$$

A.2. Spatial random effects θ

Under the Leroux CAR prior, the full conditional density of θ_i satisfies

$$f(\theta_i | \text{rest}) \propto f(\mathbf{Y} | \boldsymbol{\beta}, \boldsymbol{\theta}, \sigma^2) f(\theta_i | \boldsymbol{\theta}_{-i}, \tau^2, \rho),$$

for $i = 1, \dots, n$. Define $\bar{r}_i = m^{-1} \sum_{j=1}^m (Y_{ij} - \beta_0 - \beta_1 \mathbf{x}_{ij})$. The observations within spatial unit i contribute

$$\begin{aligned} L_i(\theta_i) &\propto \exp \left\{ -\frac{1}{2\sigma^2} \sum_{j=1}^m (Y_{ij} - \beta_0 - \beta_1 \mathbf{x}_{ij} - \theta_i)^2 \right\} \\ &= \exp \left\{ -\frac{1}{2\sigma^2} \left[\sum_{j=1}^m (Y_{ij} - \beta_0 - \beta_1 \mathbf{x}_{ij} - \bar{r}_i)^2 + m(\bar{r}_i - \theta_i)^2 \right] \right\} \\ &\propto \exp \left\{ -\frac{m}{2\sigma^2} (\theta_i - \bar{r}_i)^2 \right\}, \end{aligned}$$

where the cross term vanishes because $\sum_{j=1}^m (Y_{ij} - \beta_0 - \beta_1 \mathbf{x}_{ij} - \bar{r}_i) = 0$ by definition of \bar{r}_i . Therefore,

$$\theta_i | \text{rest} \sim \mathcal{N}(\mu_i^*, \sigma_i^{2*}),$$

where

$$\sigma_i^{2*} = \left(\frac{m}{\sigma^2} + \frac{(1-\rho) + \rho w_i}{\tau^2} \right)^{-1}, \quad \mu_i^* = \sigma_i^{2*} \left(\frac{m}{\sigma^2} \bar{r}_i + \frac{\rho \sum_{i'=1}^n w_{ii'} \theta_{i'}}{\tau^2} \right).$$

Under the nonspatial model ($\rho = 0$), the prior reduces to $\theta_i | \tau^2 \stackrel{\text{iid}}{\sim} \mathcal{N}(0, \tau^2)$, and the full conditional simplifies to

$$\theta_i | \text{rest} \sim \mathcal{N} \left(\sigma_{i,0}^{2*} \cdot \frac{m \bar{r}_i}{\sigma^2}, \sigma_{i,0}^{2*} \right), \quad \sigma_{i,0}^{2*} = \left(\frac{m}{\sigma^2} + \frac{1}{\tau^2} \right)^{-1}.$$

A.3. Error variance σ^2

Under the prior $\sigma^2 \sim \text{IG}(a, b)$, the full conditional density of σ^2 satisfies

$$\begin{aligned} f(\sigma^2 | \text{rest}) &\propto f(\mathbf{Y} | \boldsymbol{\beta}, \boldsymbol{\theta}, \sigma^2) f(\sigma^2) \\ &\propto (\sigma^2)^{-nm/2} \exp \left\{ -\frac{1}{2\sigma^2} \sum_{i=1}^n \sum_{j=1}^m (Y_{ij} - \beta_0 - \beta_1 \mathbf{x}_{ij} - \theta_i)^2 \right\} (\sigma^2)^{-(a+1)} \exp \left\{ -\frac{b}{\sigma^2} \right\} \\ &= (\sigma^2)^{-(a+nm/2+1)} \exp \left\{ -\frac{1}{\sigma^2} \left[b + \frac{1}{2} \sum_{i=1}^n \sum_{j=1}^m (Y_{ij} - \beta_0 - \beta_1 \mathbf{x}_{ij} - \theta_i)^2 \right] \right\}. \end{aligned}$$

Therefore,

$$\sigma^2 | \text{rest} \sim \text{IG} \left(a + \frac{nm}{2}, b + \frac{1}{2} \sum_{i=1}^n \sum_{j=1}^m (Y_{ij} - \beta_0 - \beta_1 \mathbf{x}_{ij} - \theta_i)^2 \right).$$

With $a = b = 0.01$, we have

$$\sigma^2 | \text{rest} \sim \text{IG} \left(0.01 + \frac{nm}{2}, 0.01 + \frac{1}{2} \sum_{i=1}^n \sum_{j=1}^m (Y_{ij} - \beta_0 - \beta_1 \mathbf{x}_{ij} - \theta_i)^2 \right).$$

A.4. Spatial variance τ^2

Because $|Q(\rho)|$ does not depend on τ^2 , under the prior $\tau^2 \sim \text{IG}(a, b)$ the full conditional density of τ^2 satisfies

$$\begin{aligned} f(\tau^2 | \text{rest}) &\propto f(\boldsymbol{\theta} | \tau^2, \rho) f(\tau^2) \\ &\propto (\tau^2)^{-n/2} \exp\left\{-\frac{\boldsymbol{\theta}^\top Q(\rho) \boldsymbol{\theta}}{2\tau^2}\right\} (\tau^2)^{-(a+1)} \exp\left\{-\frac{b}{\tau^2}\right\} \\ &= (\tau^2)^{-(a+n/2+1)} \exp\left\{-\frac{1}{\tau^2} \left(b + \frac{\boldsymbol{\theta}^\top Q(\rho) \boldsymbol{\theta}}{2}\right)\right\}. \end{aligned}$$

Therefore,

$$\tau^2 | \text{rest} \sim \text{IG}\left(a + \frac{n}{2}, b + \frac{1}{2} \boldsymbol{\theta}^\top Q(\rho) \boldsymbol{\theta}\right).$$

With $a = b = 0.01$, we have

$$\tau^2 | \text{rest} \sim \text{IG}\left(0.01 + \frac{n}{2}, 0.01 + \frac{1}{2} \boldsymbol{\theta}^\top Q(\rho) \boldsymbol{\theta}\right).$$

A.5. Spatial correlation parameter ρ

Under the prior $\rho \sim \text{Uniform}(0, 1)$, the full conditional density of ρ satisfies

$$\begin{aligned} f(\rho | \text{rest}) &\propto f(\boldsymbol{\theta} | \tau^2, \rho) \\ &\propto |Q(\rho)|^{1/2} \exp\left\{-\frac{1}{2\tau^2} \boldsymbol{\theta}^\top Q(\rho) \boldsymbol{\theta}\right\}. \end{aligned}$$

Using the spectral decomposition $L = U\Lambda U^\top$ described in Section 3.1 of the main text, and letting $\boldsymbol{\alpha} = U^\top \boldsymbol{\theta}$,

$$|Q(\rho)| = \prod_{i=1}^n (\rho\lambda_i + 1 - \rho), \quad \boldsymbol{\theta}^\top Q(\rho) \boldsymbol{\theta} = \sum_{i=1}^n (\rho\lambda_i + 1 - \rho) \alpha_i^2,$$

such that

$$\log f(\rho | \text{rest}) = \frac{1}{2} \sum_{i=1}^n \log(\rho\lambda_i + 1 - \rho) - \frac{1}{2\tau^2} \sum_{i=1}^n (\rho\lambda_i + 1 - \rho) \alpha_i^2 + \text{const.}$$

This does not correspond to a standard distribution, so ρ is updated via a Metropolis step with a Gaussian random walk proposal on the logit scale (Gamerman and Lopes 2006). Letting $\psi = \log\{\rho/(1-\rho)\}$, a proposal at iteration t is generated as $\psi^* = \psi^{(t-1)} + \eta$ with $\eta \sim \mathcal{N}(0, s^2)$, where s^2 is a tuning parameter calibrated during burn-in, and the proposal on the original scale is recovered as $\rho^* = 1/(1 + e^{-\psi^*})$. The proposal is accepted with probability $\min(1, R)$, where

$$R = \frac{f(\rho^* | \text{rest})}{f(\rho^{(t-1)} | \text{rest})} \cdot \frac{q(\psi^{(t-1)} | \psi^*)}{q(\psi^* | \psi^{(t-1)})} \cdot \frac{\rho^* (1 - \rho^*)}{\rho^{(t-1)} (1 - \rho^{(t-1)})},$$

and the proposal density ratio $q(\psi^{(t-1)} | \psi^*) / q(\psi^* | \psi^{(t-1)}) = 1$ by the symmetry of η .

Appendix B: Additional simulation results

This section provides additional simulation results for $n = 25$ and $n = 400$ spatial units. The main text presents results for $n = 100$; the figures below show that the findings are consistent across different numbers of spatial units.

B.1. Results for $n = 25$

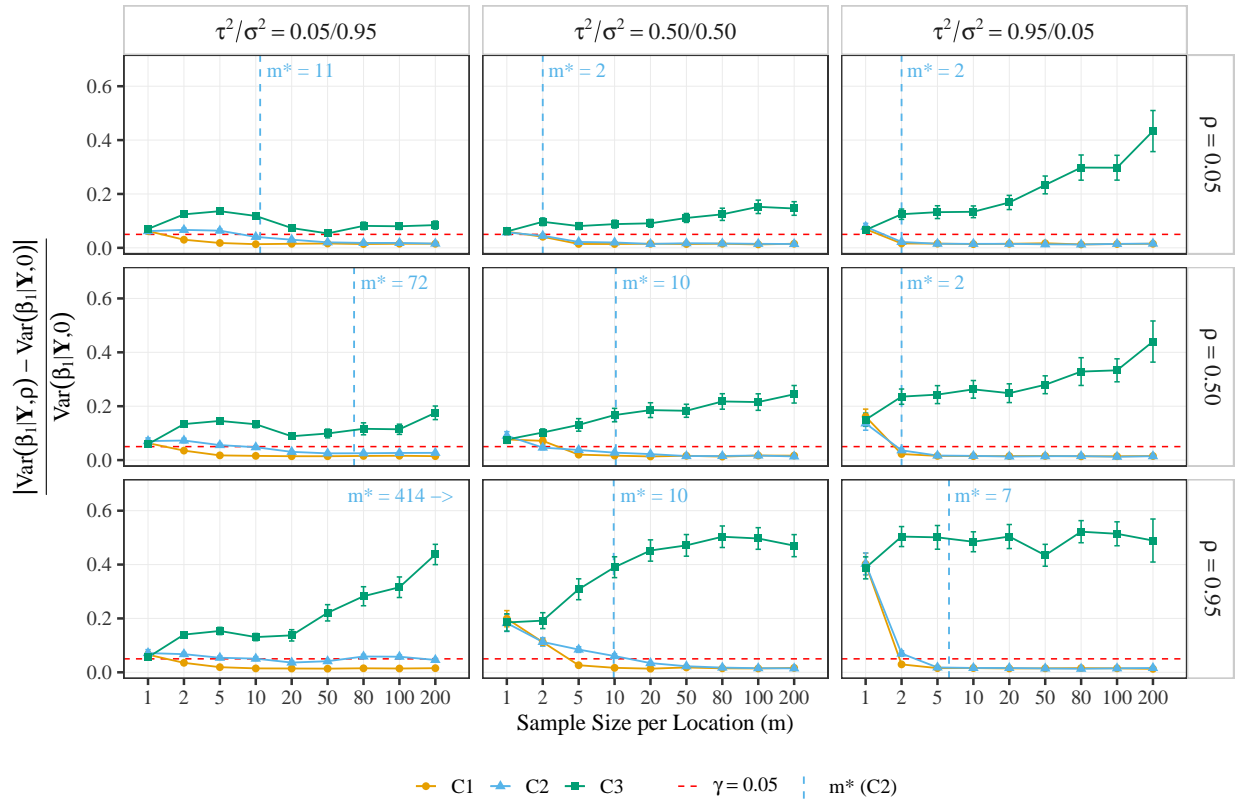


Figure B.1 Absolute relative difference in the marginal posterior variance of β_1 between the spatial (i.e., $\text{Var}(\beta_1|\mathbf{Y}, \rho)$) and nonspatial (i.e., $\text{Var}(\beta_1|\mathbf{Y}, 0)$) models, averaged over 100 datasets, for $n = 25$ spatial units. Columns correspond to the variance ratio $\kappa = \tau^2/\sigma^2$ and rows to the spatial correlation ρ . The three curves represent the three covariate structures, C1-C3, described in Table 1 of the main text. The dashed red horizontal line marks the tolerance $\gamma = 0.05$; the dashed blue vertical line marks the asymptotic bound m^* computed under C2. Error bars are pointwise 95% Monte Carlo confidence intervals across datasets.

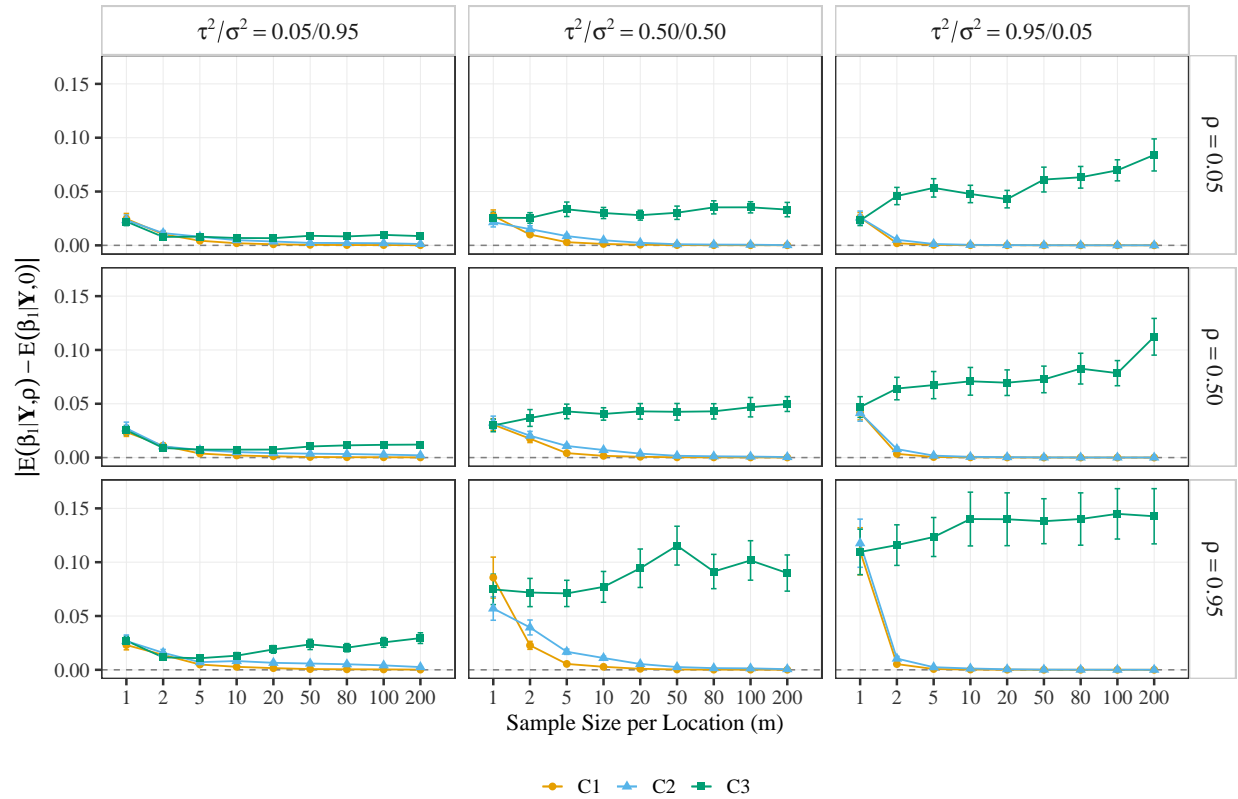


Figure B.2 Absolute difference in the marginal posterior mean of β_1 between the spatial (i.e., $E(\beta_1|\mathbf{Y}, \rho)$) and nonspatial (i.e., $E(\beta_1|\mathbf{Y}, 0)$) models, averaged over 100 datasets, for $n = 25$ spatial units. Columns correspond to the variance ratio $\kappa = \tau^2/\sigma^2$ and rows to the spatial correlation ρ . The three curves represent the three covariate structure settings, C1-C3, described in Table 1 of the main text. Error bars are pointwise 95% Monte Carlo confidence intervals across datasets.

B.2. Results for $n = 400$

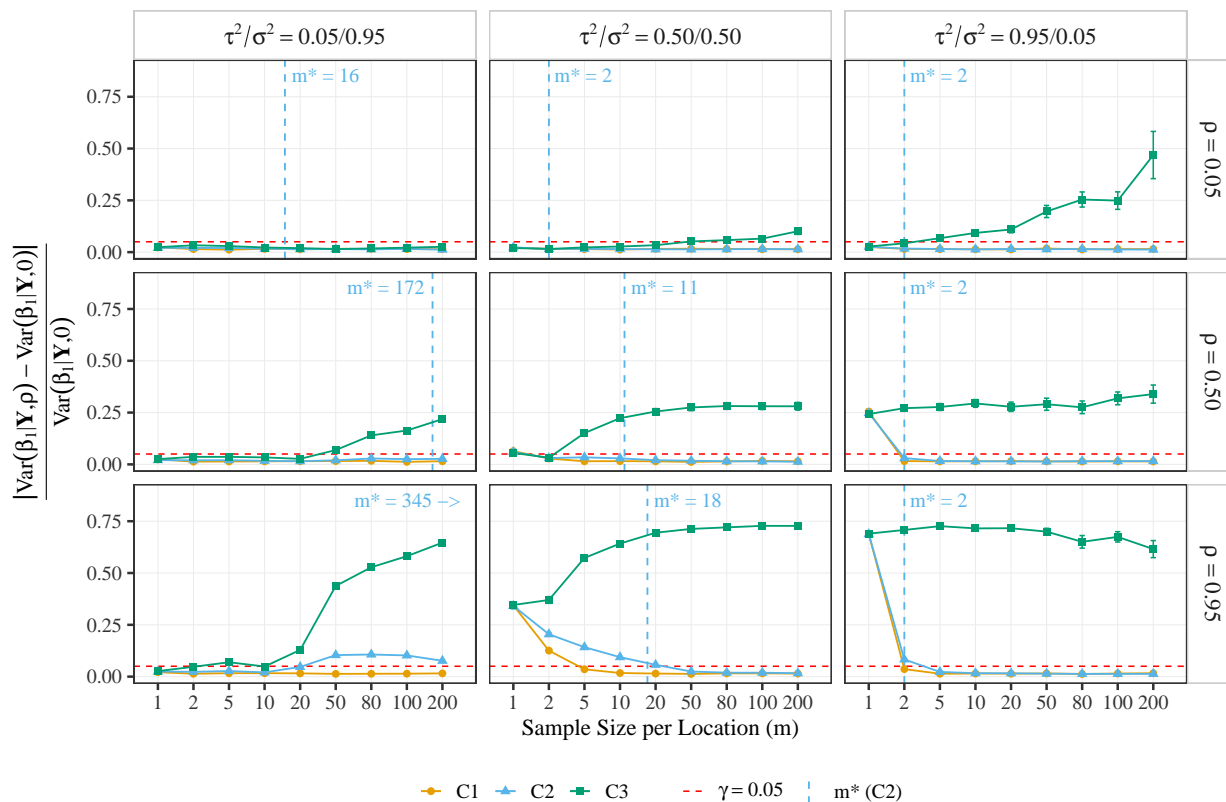


Figure B.3 Absolute relative difference in the marginal posterior variance of β_1 between the spatial (i.e., $\text{Var}(\beta_1|\mathbf{Y}, \rho)$) and nonspatial (i.e., $\text{Var}(\beta_1|\mathbf{Y}, 0)$) models, averaged over 100 datasets, for $n = 400$ spatial units. Columns correspond to the variance ratio $\kappa = \tau^2/\sigma^2$ and rows to the spatial correlation ρ . The three curves represent the three covariate structures, C1-C3, described in Table 1 of the main text. The dashed red horizontal line marks the tolerance $\gamma = 0.05$; the dashed blue vertical line marks the asymptotic bound m^* computed under C2. Error bars are pointwise 95% Monte Carlo confidence intervals across datasets.

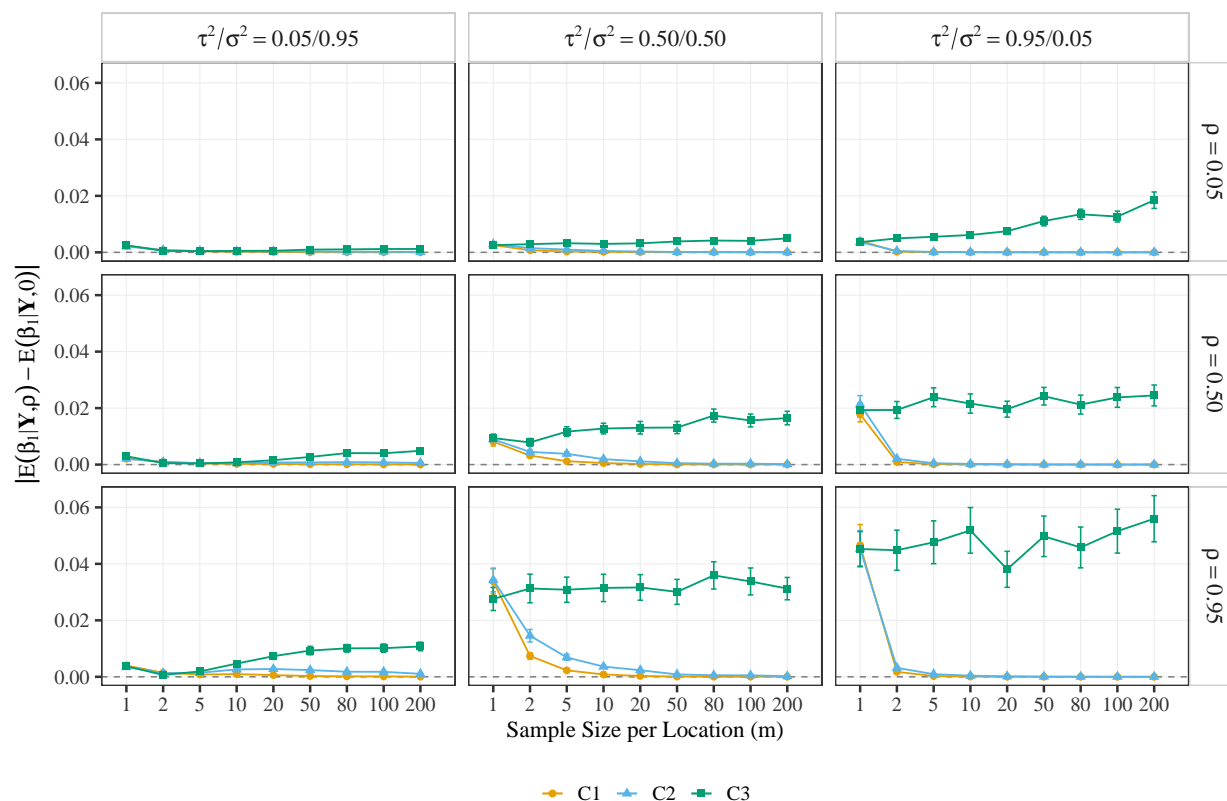


Figure B.4 Absolute difference in the marginal posterior mean of β_1 between the spatial (i.e., $E(\beta_1|\mathbf{Y}, \rho)$) and nonspatial (i.e., $E(\beta_1|\mathbf{Y}, 0)$) models, averaged over 100 datasets, for $n = 400$ spatial units. Columns correspond to the variance ratio $\kappa = \tau^2/\sigma^2$ and rows to the spatial correlation ρ . The three curves represent the three covariate structure settings, C1-C3, described in Table 1 of the main text. Error bars are pointwise 95% Monte Carlo confidence intervals across datasets.

Appendix C: Random Graph Properties

In the simulation study, each replicate uses a randomly generated connected graph as the adjacency structure. Table C.1 summarizes the degree distribution (i.e., the number of neighbors per spatial unit) across all 100 graphs generated for each value of n . The median degree is 2 across all settings, with the range of degrees increasing with n . Figure C.1 displays two example graphs for each value of n .

Table C.1 Summary of the number of neighbors per spatial unit across 100 randomly generated connected graphs for each n .

n	Mean	Median	Min	Max
25	1.920	2	1	7
100	1.980	2	1	11
400	1.995	2	1	13

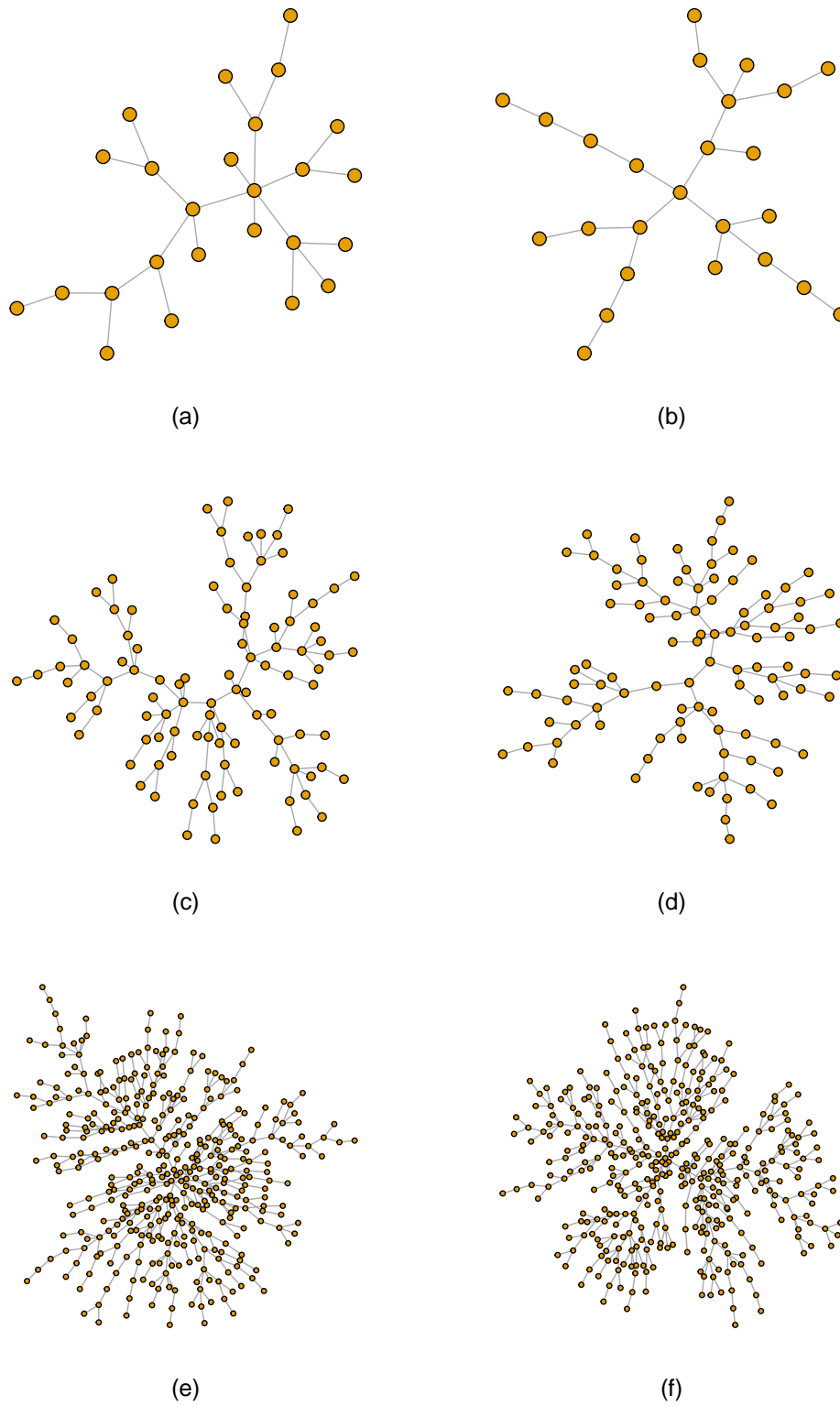


Figure C.1 Two randomly generated connected graphs used in the simulation study for (a)-(b) $n = 25$, (c)-(d) $n = 100$, and (e)-(f) $n = 400$ spatial units.